Advances in Nano Research, *Vol. 15, No. 6 (2023) 551-565*
https://doi.org/10.12989/anr.2023.15.6.551

Employing GDQ method for exploring undamped vibrational performance of CNT-reinforced porous coupled curved beam

Moein A. Ghandehari and Amir R. Masoodi*

Department of Civil Engineering, Ferdowsi University of Mashhad, Iran

(*Received May 18, 2023, Revised September 12, 2023, Accepted September 13, 2023*)

Abstract. Coupled porous curved beams, due to their low weight and high flexibility, have many applications in engineering. This study investigates the vibration behavior of coupled porous curved beams in different boundary conditions. The system consists of two curved beams connected by a mid-layer of elastic springs. These beams are made of various materials, such as homogenous steel foam, and composite materials with PMMA (polymethyl methacrylate) and SWCNT (single-walled carbon nanotube) used as the matrix and nanofillers, respectively. To obtain equivalent material properties, the role of mixture (RoM) was employed, followed by the implementation of the porosity function. The system's governing equations were obtained by employing FSDT and Hamilton's law. To investigate thermal vibration, temperature was implemented as a load in the governing equations. The GDQ method was used to solve these equations. To demonstrate the applicability of the GDQ method in calculating the frequencies of the system and the correctness of the developed program, a validation study was conducted. After validation, numerous examples were presented to investigate the behavior of single and coupled curved beams in various material properties and boundary conditions. The results indicate that the frequencies of the curved beams and the system depend highly on the amount of porosity (n) and the distribution pattern. The system frequencies decreased with an increase in the porosity coefficient. The stiffness of the springs had no effect on the first mode frequency but increased frequencies of other modes in a specific range. The frequencies of the system decreased with an increase in environmental temperature.
Keywords: carbon nano tube; coupled curved beams; natural frequency; porous beams; thermal loading

1. Introduction

Coupled-curved beam systems contain two curved beams connected with a layer of linear elastic springs. This system due to better absorption of vibration, lighter weight, higher strength, and stiffness is highly considered for engineering purposes. Coupled systems are applicable in civil, mechanical, and aerospace engineering. In civil engineering, due to specification of absorbed energy, these systems are employed to increase stability of structures in earthquakes. Another usage of coupled curved beams is in subgrade for preventing channeling and settling. The dynamic behavior of coupled beam systems is investigated in previous research (Xiaobin *et al*. 2014, Zhao *et al*. 2020, Ghandehari *et al*. 2023). In recent years, by developing new small-scale materials, application of nano and micro materials highly increased in engineering. The materials that are produced by mixing two or more materials are called composite materials. The nanocomposite materials are made of two parts: a matrix like polymer, ceramic, polyester, epoxy, or metal, and a reinforcing agent like glass fiber, carbon fiber, or aramid fiber. By using nano-composite, new materials can be produced that have desirable mechanical and chemical properties. Investigation of the dynamic behavior of composite elements became an interesting subject for researchers in recent years. Sahmani and Safaei (2022) predict microstructural- dependent three-dimensional nonlinear large-deflection composite shells, Sobhani and Masoodi (2021) investigate the vibrational behavior of doubled curved shells with paraboloidal and hyperboloidal geometries. Moreover, Rezaiee-Pajand and Masoodi (2019) peruse the nonlinear behavior of arbitrary FG shells considering large deflections and rotations.

Porous beams are a type of structural elements that is made up of a solid material with void spaces or pores within its structure. These pores can be distributed in different patterns and orientations, depending on the manufacturing process and the intended application of the beam. The porosity of a porous beam can significantly affect its mechanical properties, such as stiffness, strength, and damping. This is because the void spaces within the beam can act as stress concentrators, reducing the load-carrying capacity of the material. Numerous researches conducted to investigate the behavior of porous elements in different conditions (Ehyaei *et al*. 2017, Kitipornchai *et al*. 2017, Jouneghani *et al*. 2018, Berghouti *et al*. 2019, Ebrahimi *et al*. 2020, Fenjan *et al*. 2020, Hadji and Avcar 2021, Tlidji *et al*. 2021, Ramteke and Panda 2023, Eiadtrong *et al*. 2023). Ramteke and Panda (2023) presented a comprehensive review of the modeling and experimental challenges in porous graded structures. Jouneghani *et al*. (2018) explore the bending behavior of functionally graded (FG) nano-beams with internal porosity and subjected to a hygro-thermo-mechanical loading. Hadji and Avcar (2021) study the porous FG nanobeam by using hyperbolic shear deformation theory.

*Corresponding author, Assistant Professor,
E-mail: ar.masoodi@um.ac.ir

ISSN: 2287-237X (Print), 2287-2388 (Online)

In recent times, numerous researchers have focused on determining the natural frequencies of beams. The vibration of beam has been explored in various geometric, loading, and boundary conditions, and elastic foundations (Yas and Samadi 2012, Shen and Xiang 2013, Batihan and Kadioğlu 2016, Deng *et al*. 2017, Akbas 2018, Ebrahimi and Farazmandnia 2018, Maraş *et al*. 2018, Chaabane *et al*. 2019, Jena *et al*. 2020, Li *et al*. 2021, Babaei 2022, Hosseini *et al*. 2023). While there has been some research on the vibration behavior of coupled beams, there are only a limited number of studies that specifically investigate the vibration of homogeneous coupled beams. (Seelig and Hoppmann 1963, Rao 1974, Hamada *et al*. 1983, Oniszczuk 2000, Vu *et al*. 2000), to the authors' knowledge, there has been a lack of dedicated research aimed at exploring the potential influence of nanomaterials on the frequency behavior of these systems. This suggests that there is a significant gap in our current understanding of how the incorporation of nanomaterials may affect the vibrational response of these systems.

The GDQ method involves representing the dependent variable in terms of its values at a number of discrete points, using a set of basic functions. These basis functions are typically polynomials, and the number of points used corresponds to the number of terms in the polynomial. The GDQ method approximates the derivatives of the dependent variable at each point by taking weighted linear combinations of the values at neighboring points. The GDQ method has several advantages over other numerical techniques for solving PDEs. It is easy to implement and computationally efficient, requiring only matrix multiplications and inversions. It can also be applied to irregular domains and non-uniform grids, making it useful for a wide range of problems. In addition, the GDQ method has high accuracy and can achieve spectral convergence for smooth solutions. The GDQ method has been applied to a variety of problems in fluid dynamics, heat transfer, mechanics, and electromagnetics, among other fields. This scheme has been widely employed to peruse static and dynamic behaviors of beams, plates, and shells (Abediokhchi *et al*. 2013, Ghasemi and Mohande 2016, Li *et al*. 2017, Al-shujairi and Mollamahmutoğlu 2018, Gholami and Ansari 2018, Tang *et al*. 2018, Tornabene and Dimitri 2018, Tang and Ding 2019, Javani *et al*. 2021, Maraş and Yaman 2022, Zhang *et al*. 2022, MaraŞ and ŞEnsoy 2023, Maraş and Yaman 2023). Recently, several researches have been devoted to studying the linear and nonlinear dynamic behavior of curved beams using numerical methods (Babaei *et al*. 2019, Fariborz and Batra 2019, Salehi Kolahi *et al*. 2021).

The objective of this research is to investigate the vibration behavior of coupled curved porous beams, both non-reinforced and reinforced with carbon nanotubes, at various temperatures. The temperature distribution within the beam section is modeled using three different patterns: uniform, linear, and nonlinear. The steps followed in this research are outlined below:

1- The equivalent mechanical properties of the material including the matrix reinforced with CNTs are determined using a simple rule of mixture.

2- The function applied to the mechanical properties of the materials to model porosity in the beam section.

3- Thermal distribution function defined to model temperature distribution in three patterns.

4- The governing equation for the first shear deformation theory (FSDT) beam by applying Hamilton's principle, which takes into account thermal loading, was obtained.

5- The researchers utilize the generalized differential quadrature (GDQ) method to solve the governing equation they obtained.

6- The researchers carry out a validation study to demonstrate the accuracy and correctness of their proposed method.

7- The researchers solve several numerical examples to investigate the frequencies of systems that have materials that are not affected by temperature, as well as thermally dependent materials.

2. Coupled curved-curved beams system

In this study, the vibration behavior of the system which contains two porous curved beams investigated. These beams are connected to each other by a layer of linear springs. The geometry of beams described by *R*, radius, *L*, length, θ, central angle, and *b* and *h* are wide and height of beams section. System's boundary conditions show in the format of X-Y/x-y, in which capital letters referred to top beam and lower-case letter related to bottom beam. For instance, in a system with C-S/C-F boundary conditions, mean in top beam the left-end is clamped and the right-end is simple, and in the bottom beam, the left-end and right-end are clamped and free, respectively. Fig. 1 shows a scheme of porous system.

Assumptions considered for the system in this study are:

- Large deflections and rotations are neglected.
- The behavior of springs is linear and elastic.
- By using FDST, a thick beam can be studied.
- In-plane vibration of structures is considered.

To obtain the displacements of the system and vibration, FDST and cylindrical panel schemes are employed. The following relation is presented to obtain displacement fields of the reference layer in each curved beam.

$$\begin{aligned} D_1^i(x_i,z,t) &= d_1^i(x_i,t) + z\chi_i(x_i,t) \\ D_2^i(x_i,z,t) &= d_2^i(x_i,t) \end{aligned} \tag{1}$$

Here, D_1^i and D_2^i represented fields displacements related to longitudinal (x_i) and thickness (z) directions. d_1^i and d_2^i are displacement of mid axis in longitudinal (x_i) and thickness (z) directions. χ is a symbol that indicate the reference layer displacement. Relationship between normal and shear strain and mid-axis strain and beams curvature can be obtained by following:

$$\begin{Bmatrix} \varepsilon_x^i \\ \gamma_{xz}^i \end{Bmatrix} = \begin{bmatrix} \xi_1^i & \xi_2^i & 0 \\ 0 & 0 & \xi_2^i \end{bmatrix} \begin{Bmatrix} \varepsilon_x^{i0} \\ \Omega_x^i \\ \gamma_{xz}^{i0} \end{Bmatrix} \tag{2}$$

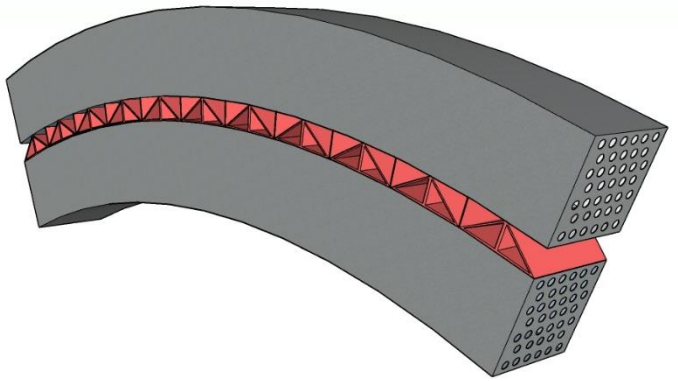

(a) general system

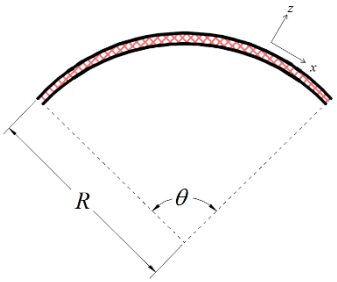

(b) definition of R and θ

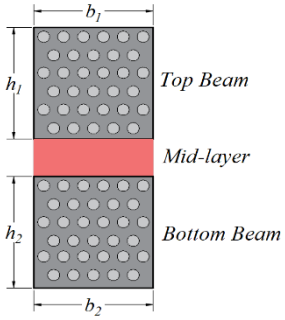

(c) system section

Fig. 1 Scheme of the system

In which,

$$\xi_1^i = \frac{1}{1+\mu_i},\ \xi_2^i = \frac{z}{1+\mu_i} \tag{3}$$

where, ε_x^i, γ_{xz}^i, ε_x^{i0} and γ_{xz}^{i0} normal strain, shear strain, normal and shear strain of neutral strain, respectively. ξ_x^i represent curvature of beams and $\mu_i = \frac{z}{R_i}$. i in these equations represent top or bottom beam in system. To find a relationship between strains and displacements of mid axis, FDST, and cylindrical panel scheme are considered.

$$\begin{Bmatrix} \varepsilon_x^{i0} \\ \xi_x^i \\ \gamma_{xz}^{i0} \end{Bmatrix} = \begin{Bmatrix} \frac{\partial}{\partial x_i} & \frac{1}{R_i} & 0 \\ -\frac{1}{R_i} & \frac{\partial}{\partial x_i} & 1 \\ 0 & 0 & \frac{\partial}{\partial x_i} \end{Bmatrix} \begin{Bmatrix} d_1^i \\ \chi_i \\ d_2^i \end{Bmatrix} \tag{4}$$

To associate stresses and strains, Hook's law is used.

$$\begin{Bmatrix} \sigma_x^i \\ \tau_{xz}^i \end{Bmatrix} = \begin{bmatrix} Q_{11} & 0 \\ 0 & Q_{55} \end{bmatrix} \begin{Bmatrix} \varepsilon_x^i \\ \gamma_{xz}^i \end{Bmatrix} \tag{5}$$

wherein, $Q_{11} = E$ and $Q_{55} = \frac{E}{2\,(1+\nu)}$. σ_x^i and τ_{xz}^i are normal stress and shear stress. E and νreferred to elastic modulus and Poisson's ratio of a porous beam, respectively. By calculating the strains, forces and moment can be obtained by employing integration of stresses in the z direction.

$$\begin{bmatrix} N_x^i \\ Q_x^i \\ M_x^i \end{bmatrix} = b_i \int_{-\frac{h_i}{2}}^{\frac{h_i}{2}} \begin{Bmatrix} \sigma_x^i \\ \tau_{xz}^i \\ z\ \sigma_x^i \end{Bmatrix} dz \tag{6}$$

The following equations can be introduced to relate the Forces and moment to reference layer strains.

$$\begin{aligned} N_x^i &= \varepsilon_x^{i0}\ A_{11}^i + \eta_x^i\ B_{11}^i \\ Q_x^i &= \gamma_{xz}^{i0}\ A_{55}^i \\ M_x^i &= \varepsilon_x^{i0}\ B_{11}^i + \eta_x^i\ D_{11}^i \end{aligned} \tag{7}$$

In which

$$\begin{aligned} A_{11}^i &= b_i \int_{-\frac{h_i}{2}}^{\frac{h_i}{2}} \phi_1^i\ E\ dz,\ B_{11}^i = b_i \int_{-\frac{h_i}{2}}^{\frac{h_i}{2}} \phi_2^i\ E\ dz \\ D_{11}^i &= b_i \int_{-\frac{h_i}{2}}^{\frac{h_i}{2}} \phi_3^i\ E\ dz,\ A_{55}^i = \kappa\ b_i \int_{-\frac{h_i}{2}}^{\frac{h_i}{2}} \phi_1^i\ \frac{E}{2(1+\nu)}\ dz \end{aligned} \tag{8}$$

Here, N_x^i, Q_x^i and M_x^i are normal and shear force and moment and $\kappa$is the shear factor which is equal to 5/6. After all, the governing equation of curved-curved system by employing Hamilton's law and Green-Gauss theory can be obtained. These equations are listed below.

$$\begin{aligned} &A_{11}^{top}\left(\frac{d^2\Phi_1}{dx^2} + \frac{1}{R_1}\frac{d\Phi_3}{dx}\right) + B_{11}^{top}\frac{d^2\Phi_2}{dx^2} \\ &+A_{55}^{top}\left(\frac{1}{R_1}\ \frac{d\Phi_3}{dx} - \frac{\Phi_1}{R_1^2} + \Phi_2\right) \\ &= I_0'\ \omega^2\ \frac{\partial^2\Phi_1}{\partial t^2} + I_1'\ \omega^2\ \frac{\partial^2\Phi_2}{\partial t^2} \end{aligned} \tag{9}$$

$$\begin{aligned} &B_{11}^{top}\ \left(\frac{d^2\Phi_1}{dx^2} + \frac{1}{R_1}\frac{d\Phi_3}{dx}\right) + D_{11}^{top}\ \frac{d^2\Phi_2}{dx^2} \\ &-A_{55}^{top}\left(\frac{d\Phi_3}{dx} - \frac{\Phi_1}{R_1} + \Phi_2\right) \\ &= I_1'\ \omega^2\ \frac{\partial^2\Phi_1}{\partial t^2} + I_2'\ \omega^2\ \frac{\partial^2\Phi_2}{\partial t^2} \end{aligned} \tag{10}$$

$$A_{55}^{top}\left(\frac{d^2\Phi_3}{dx^2}+\frac{1}{R_1}\frac{d\Phi_1}{dx}+\frac{d\Phi_2}{dx}\right)-\frac{A_{11}^{top}}{R_1}\left(\frac{d\Phi_1}{dx}+\frac{\Phi_3}{R_1^2}\right)$$
$$+\frac{B_{11}^{top}}{R_1}\left(\frac{d\Phi_2}{dx}\right)-K(\Phi_3-\Phi_6)+N_T^{top}\left(\frac{d^2\Phi_3}{dx^2}\right) \quad (11)$$
$$=I_0'\ \omega^2\ \frac{\partial^2\Phi_1}{\partial t^2}+I_1'\ \omega^2\ \frac{\partial^2\Phi_2}{\partial t^2}$$

$$A_{11}^{bottom}\left(\frac{d^2\Phi_4}{dx^2}+\frac{1}{R_2}\frac{dF_6}{dx}\right)+B_{11}^{bottom}\ \frac{d^2\Phi_5}{dx^2}$$
$$+A_{55}^{bottom}\ \left(\frac{1}{R_2}\ \frac{d\Phi_6}{dx}+\frac{1}{R_2^2}\frac{d\Phi_3}{dx}\right) \quad (12)$$
$$=I_0'\ \omega^2\ \frac{\partial^2\Phi_4}{\partial t^2}+I_1'\ \omega^2\ \frac{\partial^2\Phi_5}{\partial t^2}$$

$$A_{55}^{bottom}\left(\frac{d^2\Phi_6}{dx^2}-\frac{1}{R_1}\frac{d\Phi_4}{dx}+\frac{d\Phi}{dx}\right)$$
$$+A_{11}^{bottom}\left(\frac{1}{R_2}\ \frac{d\Phi_4}{dx}+\frac{1}{R_2^2}\frac{d\Phi_6}{dx}\right)+B_{11}^{bottom}\ \frac{1}{R_2}\frac{d\Phi_5}{dx} \quad (13)$$
$$+K_s(\Phi_6-\Phi_3)+N_T^{bottom}\left(\frac{d^2\Phi_6}{dx^2}\right)=I_0'\ \omega^2\ \frac{\partial^2\Phi_6}{\partial t^2}$$

$$B_{11}^{bottom}\ \left(\frac{d^2\Phi_4}{dx^2}+\frac{1}{R_2}\frac{d\Phi_6}{dx}\right)+D_{11}^{bottom}\frac{d^2\Phi_4}{dx^2}$$
$$-A_{55}^{bottom}\ \left(\frac{d\Phi_6}{dx}-\frac{1}{R_2}\Phi_4+\Phi_5\right) \quad (14)$$
$$=I_1'\ \omega^2\ \frac{\partial^2\Phi_4}{\partial t^2}+I_2'\ \omega^2\ \frac{\partial^2\Phi_5}{\partial t^2}$$

In these equations, $\Phi_i\ (i=1\cdots6)$ is referred to reference layer displacement for each beam, 1 to 3 for top beam and 4 to 6 related to bottom beam. I_j and I_j' obtained from below equations:

$$\{I_0,\ I_1,\ I_2,\ I_3\}\ =\ \alpha_i\ \int_{-\frac{h_i}{2}}^{\frac{h_i}{2}}\rho\ \{1,\ z,\ z^2,\ z^3\}\ dz \quad (15)$$

$$I_0'=I_0+\tfrac{I_1}{R_i},\ I_1'=I_1+\tfrac{I_2}{R_i} \quad (16)$$

N_T is the thermal load implemented to these equations and can be calculated by following:

$$N_T^J=(-b_J)\ \int_{-\frac{h_J}{2}}^{\frac{h_J}{2}}\frac{E_J\ \alpha_J\ T(z)}{1-\nu_J} \quad (17)$$

Here, E, α, and *N* are material properties of porous beam and T(z) in thermal function related to type of distribution. To solve the aforementioned equations, GDQ method is employed for solution approaches. Shu (1991) presented a method to solve partial equations in fluid mechanics and then developed for engineering practices Shu (2000). Lagrange interpolated polynomials is considered to have a simple expression for weighting coefficients. These coefficients are calculated from:

$$W_j(x)\ =\ \frac{w(x)}{(x-x_i)\ w^{(1)}(x)},\quad j=1,\ 2,\ \ldots,\ N \quad (18)$$

In which,

$$w(x)=\prod_{i=1}^{N}(x-x_i),$$
$$w^{(1)}(x)=\prod_{i=1,\ i\neq j}^{N}(x_j-x_i) \quad (19)$$

For the first and higher order of derivation, weighting coefficients can be obtained by employing the following equations. For the first order:

$$c_{ji}^{(1)}=\begin{cases}\dfrac{w^{(1)}(x_j)}{(x_j-x_i)\ w^{(1)}(x_j)}, & when\ \ i\neq j\\ \displaystyle\sum_{k=1,\ j\neq k}^{N}c_{jk}^{(1)}, & when\ \ i\neq j\end{cases} \quad (20)$$

where,

$$w^{(1)}(x_j)\ =\ \prod_{i=1,\ j\neq i}^{N}(x_j-x_i),\quad i=j=1,\ 2,\ \ldots,\ N \quad (21)$$

And for the higher order of derivation:

$$c_{ji}^{(n)}=\begin{cases}n\left(c_{jj}^{(n-1)}\ c_{ji}^{(1)}-\dfrac{c_{ji}^{(n-1)}}{x_j-x_i}\right), & when\ \ i\neq j\\ \displaystyle\sum_{k=1,\ j\neq k}^{N}c_{jk}^{(n)}, & when\ \ i\neq j\end{cases} \quad (22)$$

To import boundary conditions, the direct way is employed. Grid points related to the BCs are removed and the effect of them on other grid points (internal points) is ignored. The mathematical appearance of BCs is given as follows:

$$\text{For C-C: } d_1^i=d_2^i=\chi_i=0$$
$$\text{For S-S: } d_1^i=d_2^i=M_x^i=0 \quad (23)$$
$$\text{For F-F: } N_x^i=Q_{xz}^i=M_x^i=0$$

The natural frequencies of the system are calculated by using the flowing expression:

$$\left|D_{eff}-\omega^2\ M_{eff}\right|=0 \quad (24)$$

Here, D_{eff} and M_{eff} are effective stiffness and mass matrices related to internal points. These matrices can be obtained from:

$$\left[D_{eff}\right]=[D_I]-[D_{IB}]\ [D_B]^{-1}[D_{BI}] \quad (25)$$

$$\left[M_{eff}\right]=[M_I] \quad (26)$$

wherein, D_I is stiffness matrix related to internal points, D_{IB} is internal stiffness matrix associated with BCs and D_B is BCs matrix stiffness. M_I define as mass matrix related to the internal points.

3. Functionally graded porous beam reinforced by CNTs

To model a CNT reinforced porous beam, firstly CNTs must be modeled in a beam section. Several methods have

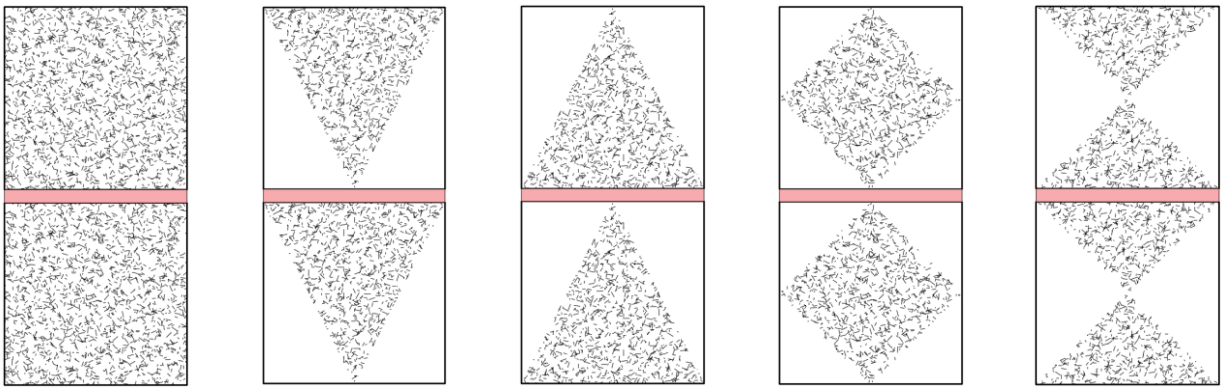

(a) (b) (c) (d) (e)

Fig. 2 Different types of CNTs distribution throughout beam section, a) uniform, b) V pattern, c) pattern, d) O pattern, and e) X pattern

Table 1 The function of CNTs distribution

Pattern Type	Distribution Factor (μ)
UD	1
FG-V	$\left(1+2\frac{z}{h}\right)$
FG-	$\left(1-2\frac{z}{h}\right)$
FG-O	$4\left(0.5-\frac{\lvert z\rvert}{h}\right)$
FG-X	$(4\left(\frac{\lvert z\rvert}{h}\right))$

been proposed to determine the equivalent properties of CNT-reinforced beams. In this study, the role of mixture (RoM) is employed to simply calculate equivalent materials. The following relations are presented in (Han and Fina 2011, Yas and Samadi 2012, Song *et al*. 2016, Ghandehari *et al*. 2023).

$$V_r + V_M = 1 \tag{27}$$

$$V_r = \mu V_{CN} \tag{28}$$

$$E_R^{11} = \eta_1\ V_r E_{CN}^{11} + V_M E_M \tag{29}$$

$$E_R^{22} = \frac{\eta_2}{\frac{V_r}{E_{CN}^{22}} + \frac{V_M}{E_M}} \tag{30}$$

$$G_R^{12} = \frac{\eta_3}{\frac{V_r}{G_{CN}^{12}} + \frac{V_M}{G_M}} \tag{31}$$

$$\upsilon_R = \upsilon_{CN}\ V_r + \upsilon_M\ V_M \tag{32}$$

$$\rho_R = \rho_{CN}\ V_r + \rho_M\ V_M \tag{33}$$

$$\kappa_R = \kappa_{CN}\ V_r + \kappa_M\ V_M \tag{34}$$

$$\alpha_R = \frac{V_r E_{CN}^{11}\ \alpha_{CN} + V_M E_M\ \alpha_M}{V_r E_{CN}^{11} + V_M E_M} \tag{35}$$

Which, V_M and V_{CN} are the volume of matrix and CNTs in beam, respectively. The Young's and shear moduli of the CNTs are denoted by E_{CN}^{11}, E_{CN}^{22} , and G_{CN}^{12}, respectively. E_M and G_M referred to the Young's and shear modulus of matrix. $\eta_i(i = 1,2,3)$ are size-dependent material properties and related to the value of V_{CN}. Additionally, κ s the equivalent thermal conductivity of the CNT-reinforced beam. μ is a function that describes the distribution of the CNTs throughout the beam section. α_R, α_{CN}, and α_M are the thermal expansion coefficient of nanocomposite, CNTs, and matrix, respectively. In the present study, five types of CNTs patterns are considered. Table 1 shows the functions of CNTs patterns and Fig. 2 indicated the pattern of distribution.

Upon completion of the equivalent materials calculations, the subsequent task involves the modeling of porosity within the beam section. This pivotal stage seeks to derive Young's modulus E(z), shear modulus G(z), density ρ(z), and thermal conductivity κ(z) of the porous carbon nanotubes (CNTs) beam through algorithmic formulations as demonstrated below (Chen *et al*. 2016, Kitipornchai *et al*. 2017, Eiadtrong *et al*. 2023):

$$E(z) = E_R^{11}\ \{1 - n_0\ \psi(z)\} \tag{35}$$

$$G(z) = G_R^{12}\ \{1 - n_0\ \psi(z)\} \tag{36}$$

$$\rho(z) = \rho_R\ \{1 - n_m\ \psi(z)\} \tag{37}$$

$$\kappa(z) = \kappa_R\ \{1 - n_m\ \psi(z)\} + \kappa_{air}\ \{n_m\ \psi(z)\} \tag{38}$$

The coefficient n_0 is crucial in the determination of the porosity present in a given beam section. Meanwhile, the coefficient n_m can be computed using the mechanical property expression of closed-cell cellular solids subject to a Gaussian Random Field (GRF) [8]. This calculation method establishes the relationship between the distribution of the material property of the cellular solids and the corresponding density of pores across the beam section. The GRF formula utilized provides a probabilistic framework for describing the likelihood of particular values of nm while taking into account the inherent variability that is present in the material structure. By employing this methodology, a more precise and accurate analysis of the porosity in the beam section can be achieved.

$$n_m = \frac{1.121\ \left\{1 - \sqrt[2.3]{1 - n_0\ \psi(z)}\right\}}{\psi(z)} \tag{39}$$

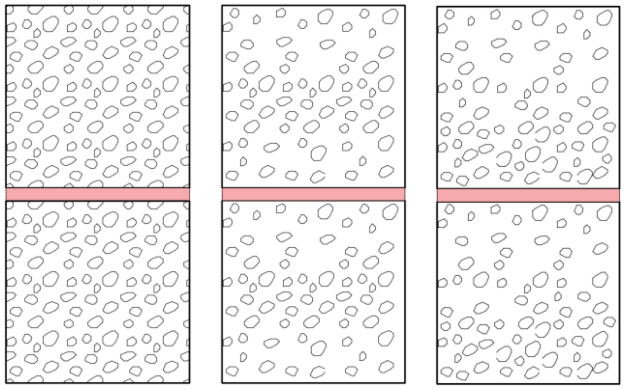

(a) (b) (c)

Fig. 3 Pattern of porosity distribution in the system section, a) uniform, b) symmetric, and c) asymmetric

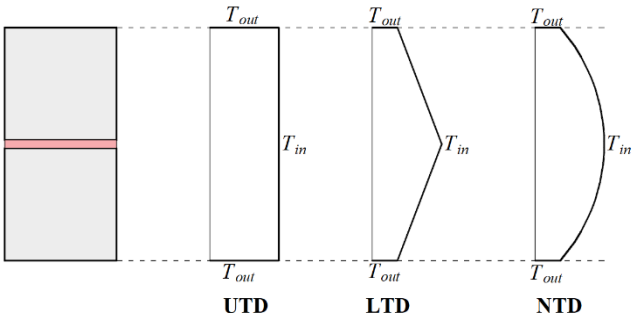

Fig. 4 The scheme of thermal distribution in the system section

Based on the closed-cell GRF scheme, Poisson's ratio can be calculated based on (Roberts and Garboczi 2002):

$$\upsilon(z) = 0.221\ \Theta + \upsilon_R(0.342\ \Theta^2 - 1.21\ \Theta + 1) \quad (40)$$

where,

$$\Theta = 1 - \frac{\rho(z)}{\rho_R} = 1.21\ \left\{1 - \sqrt[2.3]{1 - n_0\ \psi(z)}\right\} \quad (41)$$

ψ(z) is a z-function which describes the distribution of porosity in beam section. In this study, three types of uniform (PUD), symmetric (PSD), and asymmetric pattern (PAD) are considered for porosity distribution. The functions of the patterns are:

$$\psi(z) = \begin{cases} 1 & , Uniform\ Distribution \\ cos\left(\frac{\pi z}{h}\right) & , Symmetric\ Distribution \\ cos\left(\frac{\pi z}{h} + \frac{\pi}{4}\right) & , Asymmetric\ Distribution \end{cases} \quad (42)$$

To investigate how temperature affects the frequencies of a system, three different thermal distributions were utilized: uniform distribution (UTD), linear distribution (LTD), and non-linear distribution (NTD). The mathematical formulations for these thermal distributions are presented below (Chen *et al*. 2018, Eiadtrong *et al*. 2023):

$$\text{UTD: } T(z) = T_0 + \Delta T \quad (43)$$

$$\text{LTD: } T(z) = T_{bot} + \left(T_{top} - T_{bot}\right)\left(\frac{h+2z}{2h}\right) \quad (44)$$

$$\text{NTD: } T(z) = T_{bot} + \frac{(T_{top} - T_{bot})}{\int_{-\frac{h}{2}}^{\frac{h}{2}}\{1/\kappa(z)\}dz}\left[\int_{-\frac{h}{2}}^{z}\{1/\kappa(z)\}dz\right] \quad (45)$$

4. Validation

In this study, a computer program is developed to calculate the natural frequencies of coupled curved-curved CNT beam. To validate the accuracy of the program, various examples from previous studies were solved and their results were compared. One such study by Rezaiee-Pajand and Rajabzadeh-Safaei (2016) investigated the dynamic behavior of a curved beam using FEM and calculated the natural frequencies under different boundary conditions. The dimensions of the beam for simple-simple and clamped- clamped boundary conditions were as stated before. The geometry of beam with Simple-Simple (S-S) BCs are R=0.75 m, A=4 m^2, I=0.01 m^4, and R/h=4 and for clamped-clamped boundary condition are R=0.6366 m, A=1 m^2, I=0.0016 m^4 and R/h=6. The materials properties of structure are E=70 GPa, *N*=0.4166, ρ=2777 kg/m^3, and κ=0.85. Table 3 shows the frequency of curved beam obtained in this research and compares the results with the results of Rezaiee-Pajand and Rajabzadeh-Safaei (2016). Frequencies calculated by this program are close to the value obtained in (Rezaiee-Pajand and Rajabzadeh-Safaei 2016).

Sobhani and Masoodi (2023) study the vibration behavior of coupled curved-curved beams that are connected by a layer of springs in different boundary conditions. The findings of Sobhani and Masoodi (2023) are supported by Table 3, which confirms the this research results through compression. The geometry properties of beams in (Sobhani and Masoodi 2023) are L_i=10 R_1=R_2=7.5 and h_1=h_2=b_1=b_2=0.1. Material properties are E=200 GPa, *N*=0.34, ρ=7850 kg/m^3, κ=0.87 and mid-layer stiffness is 16×10^3. The frequencies calculated for this situation are in the range of frequencies calculated by (Sobhani and Masoodi 2023).

Chen *et al*. (2016) investigate the free and forced vibration characteristics of the foundationally graded porous beam in different boundary conditions. Table 4 indicates the results of (Chen *et al*. 2016) and this study's results to compare and validate the developed program. Two types of porosity distributions - symmetric and asymmetric patterns - were employed with a porosity of 0.5 for the beams. The materials proprietaries considered for beam are E_1=200 GPa, ρ_1=7850 kg/cm^3, and *N*=1/3 The boundary conditions are C-C, S-S, C-S, and C-F and the slenderness ratio of beam are varied from 10 to 50. The results of Chen *et al*. (2016) of indicate that the porosity of beams has a significant impact on the free and forced vibration characteristics of the beams. By comparing the results, the capability of GDQ method in calculating the frequencies of porous beam is assessed.

Eiadtrong *et al*. (2023) investigate the thermal vibration of straight beam by employing modified Fourier method. Table 5 shows the non-dimension frequencies obtained

Table 2 Dimensionless frequency of the homogenous curved beam

mode	S-S		C-C	
	This study	Rezaiee-Pajand and Rajabzadeh-Safaei (2016)	This study	Rezaiee-Pajand and Rajabzadeh-Safaei (2016)
1	29.2757	29.2850	36.7045	36.7160
2	33.2995	33.3210	42.2656	42.2780
3	67.1136	67.2020	82.2368	82.3610
4	79.9578	80.0490	84.4943	84.5650
5	107.835	108.169	122.311	122.722

Table 3 Natural frequencies of coupled homogenous curved beams

mode	C-C/C-C		S-S/S-S	
	This study	Sobhani and Masoodi (2023)	This study	Sobhani and Masoodi (2023)
1	10.931	10.932	6.7019	6.7023
2	11.342	11.342	7.3345	7.3349
3	20.620	20.621	15.545	15.546
4	20.860	20.861	15.860	15.861
5	37.380	37.382	29.528	29.530

Table 4 Dimensionless frequencies of straight beam with different BCs and slenderness ratio (n=0.5 and $\omega L\sqrt{I_m/A_m}$)

BCs	L/h	Porosity distribution					
		Symmetric			Asymmetric		
		This Study	Chen *et al*. (2016)	Chen *et al*. (2016) (ANSYS)	This Study	Chen *et al*. (2016)	Chen *et al*. (2016) (ANSYS)
S-S	10	0.2624	0.2798	0.2778	0.2515	0.2599	0.2549
	20	0.1320	0.1422	0.1419	0.1266	0.1318	0.1296
	50	0.0529	0.0571	0.0571	0.0507	0.0529	0.0521
C-C	10	0.5924	0.5944	0.6101	0.5430	0.5475	0.5600
	20	0.3087	0.3166	0.3176	0.2812	0.2888	0.2941
	50	0.1250	0.1291	0.1289	0.1137	0.1174	0.1183

from (Eiadtrong *et al*. 2023) and current study. In both studies, beam are made by steel foam with following properties: E_1=200 GPa, ρ_1 =7850 kg/cm^3, κ_1 = 12.143 W/mK, α_1= 15.321×10^6 1/K and $G_1=E_1/[2(1+N)]$. The thermal conductivity of air assumes to be 0.025 W/mk. The geometry of beams is L/h=20 and h=b, and boundary conditions is clamped at both ends. Porosity is distributed with three patterns of uniform, symmetric, and asymmetric throughout beam section and initial porosity is 0.5. Furthermore, this table provides a good insight into the convergence of GDQ method in calculating frequencies. $\omega L\sqrt{I_m/A_m}$is employed to obtain dimensionless frequencies, in which $A_m = b\int_{-\frac{h}{2}}^{\frac{h}{2}}\frac{E}{1-\nu^2}\,dz$ and $I_m = b\int_{-\frac{h}{2}}^{\frac{h}{2}}\rho\,dz$.

Table 6 shows the effect of uniform thermal distribution on frequencies of beam. The materials properties are like the previous example. The beam geometry properties are L/h=10 and L=h. Dimensionless frequencies are obtained for C-S and S-S boundary conditions. The temperature throughout beam is uniformly distributed and ΔT is assumed to be zero, 100, and 200. Different porosity is employed to study the effect of porosity on frequencies of beam.

5. Numerical examples

In previous section, the capability of program in calculating the frequencies of single and double curved and straight beams are shown. The aim of this section is to investigate the natural frequencies of double and single curved beams in various porosity and CNTs patterns. In the first example, the effect of R/h on the dimensionless frequencies of porous and non-porous beam was investigated. Fig. 5, shows the first dimensionless frequency of a single beam in various boundary conditions. The beam is made of steel foam and the material properties are E= 200 GPa, ρ=7850 kg/m^3, N=1/3, κ_1= 12.143 W/mK, α= 15.321 ×10^{-6}. The thermal conductivity of air is κ_{air}= 0.025 W/mK. The temperature is assumed to be 300 K and uniformly

Table 5 Dimensionless frequencies of straight beam with clamped BCs in both ends (L/h=20, n_0= 0.5, and $\omega L\sqrt{I_m/A_m}$)

Eiadtrong *et al*. (2023) (Modified Fourier Method)						
Porosity Distribution	Modes	Node				
		5	10	15	20	25
Uniform	1	0.2850	0.2847	0.2846	0.2846	0.2847
	2	0.7813	0.7644	0.7643	0.7643	0.7646
	3	1.4815	1.4538	1.4513	1.4511	1.4518
Symmetric	1	0.3143	0.3141	0.3141	0.3141	0.3142
	2	0.8503	0.8367	0.8367	0.8367	0.8371
	3	1.6038	1.5764	1.5749	1.5746	1.5757
Asymmetric	1	0.2880	0.2877	0.2876	0.2876	0.2877
	2	0.7888	0.7721	0.7720	0.7720	0.7723
	3	1.4953	1.4676	1.4652	1.4650	1.4657
This Study (GDQ Method)						
Porosity Distribution	Modes	Node				
		5	7	9	11	15
Uniform	1	0.2728	0.2698	0.2699	0.2699	0.2699
	2	2.6654	0.7711	0.7278	0.7278	0.7278
	3	2.7020	1.4824	1.3873	1.3879	1.3877
Symmetric	1	0.3024	0.2991	0.2992	0.2992	0.2992
	2	2.7050	0.8499	0.8040	0.8039	0.8039
	3	2.7452	1.6257	1.5256	1.5263	1.5261
Asymmetric	1	0.2758	0.2727	0.2728	0.2728	0.2728
	2	2.7038	0.7797	0.7358	0.7358	0.7358
	3	2.7432	1.4990	1.4027	1.4032	1.4031

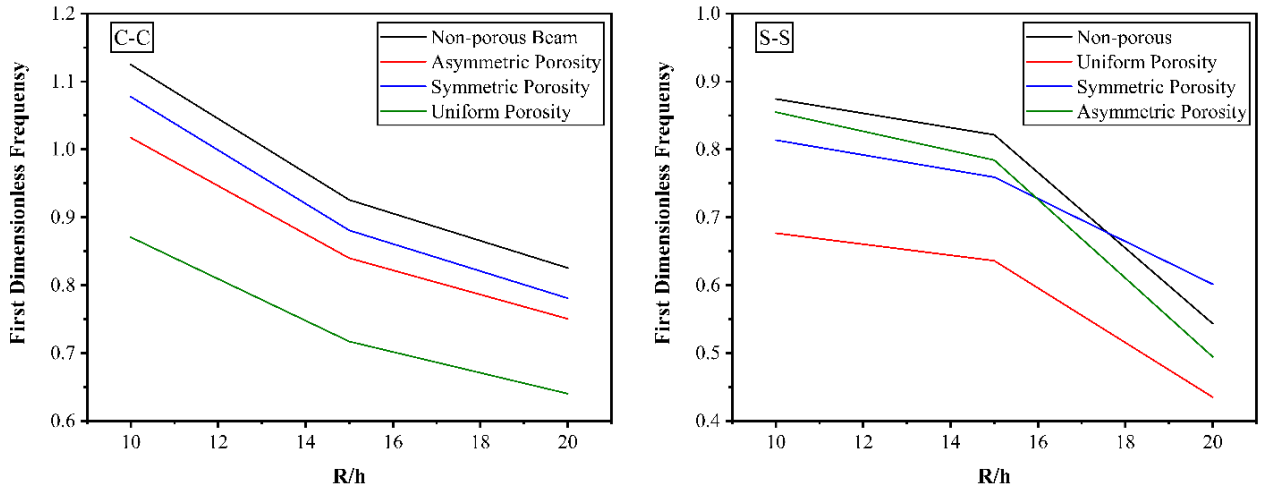

(a) both ends are clamped (b) both ends are simple

Fig. 5 The effect of radius to height ratio on the first dimensionless frequency of a single curved beam in different porosity pattern

distributed in beam section. The geometry of beam is R= 10, θ=45°, L=2×R×sin (θ/2), and dimension-less frequencies are obtained by using $\omega L\sqrt{I_m/A_m}$.

Porosities are distributed with three different patterns, uniform, symmetric, and asymmetric and n_0 is 0.5. Based on this figure, beam's frequencies decrease by increasing in R/h ratio. It means that an increase in the height of the beam section causes frequencies to increase.

To assess the effect of porosity on the dimensionless frequencies of curved beam, the following Fig. 6 is

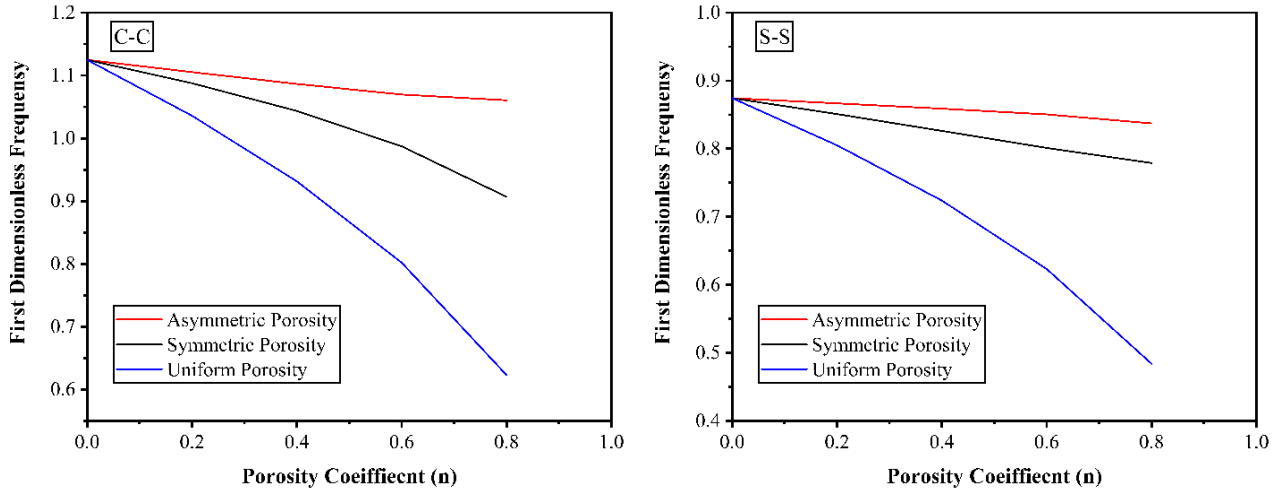

(a) C-C (b) S-S

Fig. 6 Investigation of the effect of porosity on the frequencies of system for various porosity pattern in different boundary conditions

Table 7 Mechanical properties of SWCNTs (10,10) and PMMA

Item	Value	Unite
SWCNT (10,10) (Yu *et al*. 2005, Sobhani and Masoodi 2023)		
E_{11}^{CNT}	600	GPa
E_{22}^{CNT}	10	GPa
G_{12}^{CNT}	17.2	GPa
υ_{CNT}	0.19	---
ρ_{CNT}	1400	kg/m^3
κ_{CNT}	2000	W/mK
α_{CNT} (at 300^o K)	3.4584×10^{-6}	---
PMMA (Elimat *et al*. 2008, Sobhani and Masoodi 2023)		
E^{Matrix}	2.5	GPa
ρ_{Matrix}	1190	kg/m^3
κ_{m}	0.168	W/mK
α_{m} (at 300^o K)	45×10^{-6}	---

presented. The material properties of this example are the same as previous section and the beam geometry is R/h= 10, R= 10, θ=45^o. Uniform, symmetric, and asymmetric patents are employed for distribution of porosity throughout beam section. The porosity coefficient (n) varied from zero to 0.8. Like the previous example, in this part, the environment temperature is assumed to be 300^o K. As can be seen, increase in the porosity coefficient causes the frequencies of beam decrease. Furthermore, a beam with asymmetric porosity has greater frequency values than other patterns. For frequencies based on the porosity pattern can be said:

Asymmetric > Symmetric > Uniform

At R/h=15, a pivotal shift occurs in how R/h influences the beam's frequencies. For C-C boundary conditions, after reaching this value, the effect of frequencies due to changes in R/h mainly diminishes. However, under S-S boundary conditions, when R/h holds a greater value, it exerts a more significant influence on frequencies compared to values smaller than R/h=15.

The frequencies of single porous curved beam reinforced with CNTs are presented in Fig. 7. The material properties of matrix and CNTs have shown in Table 7. The geometry of beam is the same as previous section and porosity is uniformly distributed throughout beam section. Three different volumes of CNTs are considered, 0.12, 0.17, and 0.28 which indicate low, medium, and high volume of CNTs, respectively. The UD (uniform distributed) pattern is employed for distribution of CNTs in beam section. According to this Fig., first dimensionless frequency of curved beam decreased with an increase in porosity coefficient and increased with an increase in volume of CNTs.

In previous parts, the vibration behavior of porous curved beam reinforced by CNTs investigate. In the following, the dynamic behavior of coupled curved porous beam with a linear springs' mid-layer is discussed. Firstly, the effect of R/h is investigated. Fig. 8, presented the first dimensionless frequencies for different R/h value in S-S/S-S and C-C/C-C boundary conditions. The beam is made of PMMA and reinforced with SWCNTs. The materials properties are mentioned in Table 7. The geometry of beams is R=10, θ=45^o. Porosity is distributed in beam section by three different patterns, uniform, symmetric and asymmetric. CNTs uniformly distributed throughout beam and the volume of CNTs is assumed to be 0.17. The environments temperature is assumed to be room temperature (300^o K). The stiffness of spring (K) is defined as coefficient $\int \frac{E}{2\,L^2(1-\nu)}\,dz$, which E and N referred to as matrix properties. It is worth to mentioned that the geometry and material properties in both beams are the same. Results indicate that for non-porous and porous system, frequencies decreased with an increase in the R/h ratio. This is because increasing the R/h results in a decrease in the stiffness of the beam, in which turn leads to a decrease in the natural frequency of the beam.

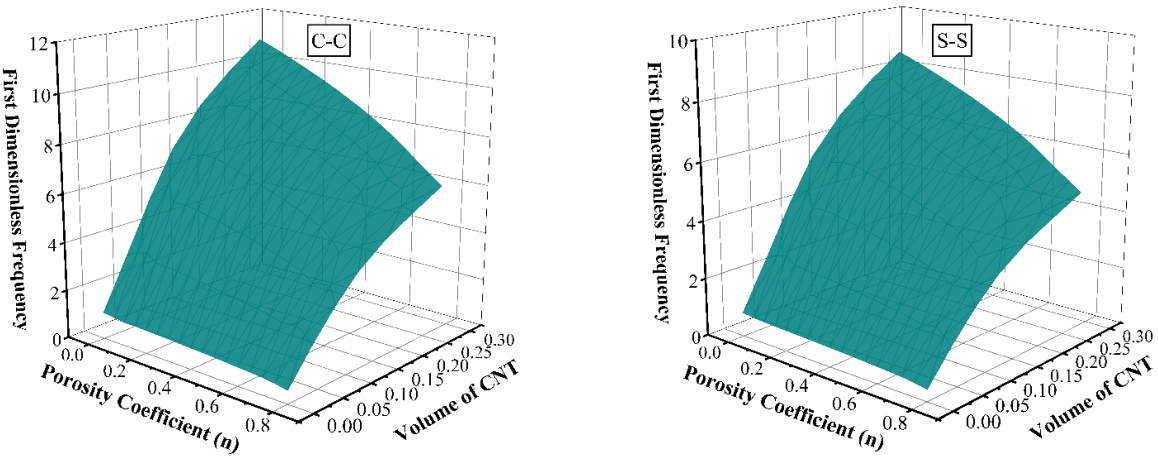

(a) C-C boundary condition (b) S-S boundary condition

Fig. 7 Frequencies of porous curve beam reinforced by CNTs in various porosity coefficient

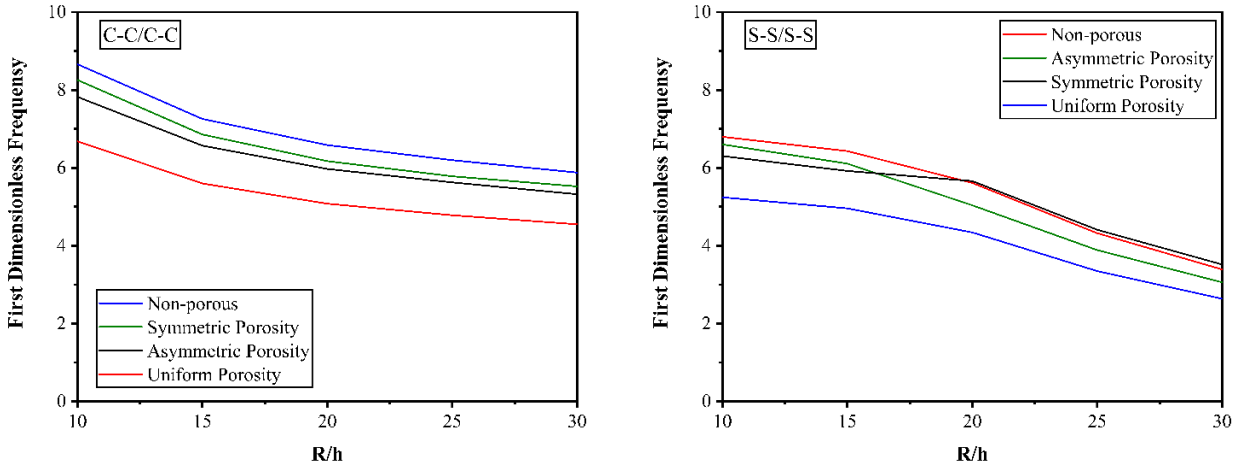

(a) C-C/C-C (b) S-S/S-S

Fig. 8 The effect of R/h on the frequencies of system in different porosity distribution

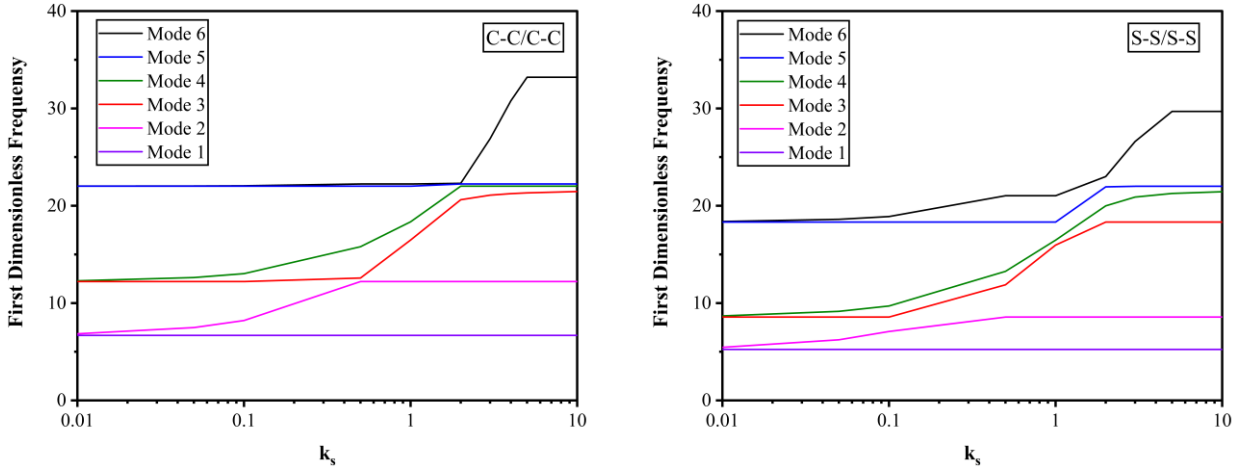

(a) C-C/C-C (b) S-S/S-S

Fig. 9 Investigation about the influence of K on the various modes of the system with porous beam (n= 0.5) reinforced with CNTs (V_{CNT}= 0.17)

The system consists of two curved beams and a spring mid-layer. To assess the effect of spring stiffness on the system's frequencies, Fig. 9 is presented. The porous beams in this system are made of PMMA and reinforced with

Table 8 The effect of thermal distribution and temperature increase on the vibration behavior of the system

BCs	Thermal Distribution	T_{out}	T_{in}	Modes				
				1	2	3	4	5
C-C	Constant	300	300	6.6834	12.210	21.460	22.014	22.232
		500	500	6.6344	12.124	21.460	22.008	22.126
		700	700	6.5848	12.037	21.460	22.002	22.022
		900	900	6.5352	11.951	21.458	21.916	21.998
	Linear	300	300	6.6834	12.210	21.460	22.014	22.232
		300	500	6.6590	12.167	21.460	22.010	22.010
		300	700	6.6344	12.124	21.460	22.008	22.126
		300	900	6.6100	12.081	21.460	22.006	22.074
	Non-linear	300	300	6.6834	12.210	21.460	22.014	22.232
		300	500	6.6590	12.167	21.460	22.010	22.180
		300	700	6.6344	12.124	21.460	22.008	22.126
		300	900	6.6100	12.081	21.460	22.006	22.074
S-S	Constant	300	300	5.2426	8.5584	18.319	21.442	22.002
		500	500	5.1918	8.4440	18.197	21.442	21.998
		700	700	5.1400	8.3278	18.074	21.442	21.994
		900	900	5.0884	8.2096	17.949	21.442	21.990
	Linear	300	300	5.2426	8.5584	18.319	21.442	22.002
		300	500	5.2170	8.5012	18.258	21.442	22.000
		300	700	5.1918	8.4440	18.197	21.442	21.998
		300	900	5.1662	8.3856	18.135	21.442	21.996
	Non-linear	300	300	5.2426	8.5584	18.319	21.442	22.002
		300	500	5.2170	8.5012	18.258	21.442	22.000
		300	700	5.1918	8.4440	18.197	21.442	21.998
		300	900	5.1662	8.3856	18.135	21.442	21.996
BCs	Thermal Distribution	T_{in}	T_{out}	Modes				
				1	2	3	4	5
C-C	Linear	300	300	6.6834	12.210	21.460	22.014	22.232
		300	500	6.6590	12.167	21.460	22.010	22.010
		300	700	6.6344	12.124	21.460	22.008	22.126
		300	900	6.6100	12.081	21.460	22.006	22.074
	Non-linear	300	300	6.6834	12.210	21.460	22.014	22.232
		300	500	6.6590	12.167	21.460	22.010	22.180
		300	700	6.6344	12.124	21.460	22.008	22.126
		300	900	6.6100	12.081	21.460	22.006	22.074
S-S	Linear	300	300	5.2426	8.5584	18.319	21.442	22.002
		300	500	5.2170	8.5012	18.258	21.442	22.000
		300	700	5.1918	8.4440	18.197	21.442	21.998
		300	900	5.1662	8.3856	18.135	21.442	21.996
	Non-linear	300	300	5.2426	8.5584	18.319	21.442	22.002
		300	500	5.2170	8.5012	18.258	21.442	22.000
		300	700	5.1918	8.4440	18.197	21.442	21.998
		300	900	5.1662	8.3856	18.135	21.442	21.996

CNTs with a volume fraction of 0.17. A porosity coefficient of 0.5 is assumed to model semi-porous beams. CNTs and porosity are uniformly distributed in both beam sections. The beam geometry has a radius of 10, a radius-to-thickness

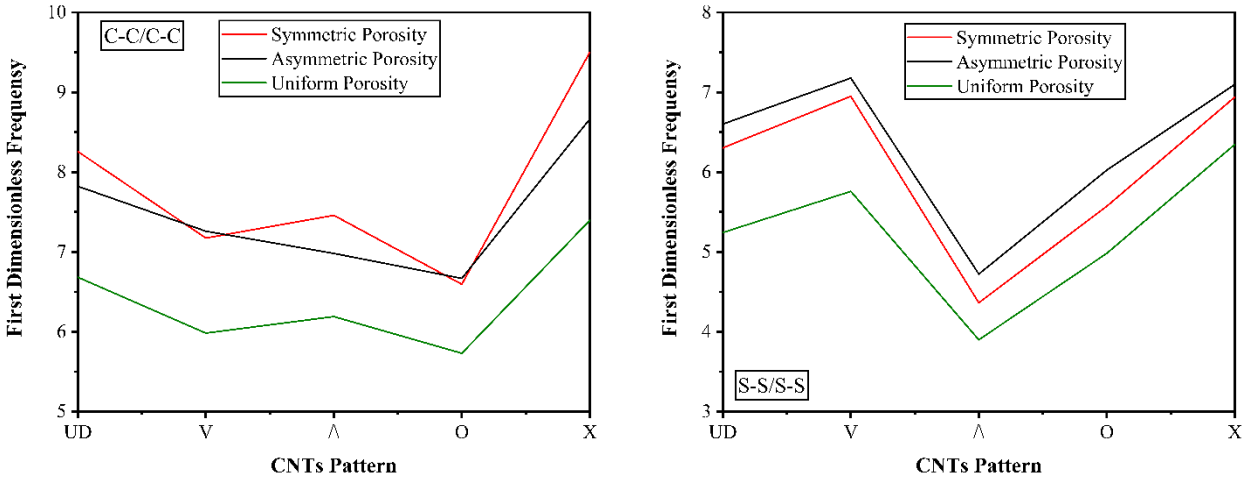

(a) C-C/C-C (b) S-S/S-S.

Fig. 10 The relation between CNTs pattern, porosity distribution, and frequency of the porous system

ratio of 10, and an angle of 45 degrees. As mentioned before, the spring coefficient is defined as a factor of the matrix modulus and Poisson's ratio. To cover a wide range of K, the spring stiffness coefficient (ks) is assumed to vary from 0.01 to 100. Based on Fig. 9, spring stiffness has no effect on the first mode frequency. In other modes, frequencies remain constant until a specific value of ks, after which they increase to a maximum value. This suggests that a specific range of K values affects the system's frequencies. The range of K values that cause a change in frequencies by increasing K is related to the number of modes and boundary conditions.

Furthermore, the effect of porosity and CNTs pattern on the frequencies of the system was investigated. The geometry and material properties are the same as previous section. Five different CNTs patterns and three porosity patterns were considered. The mid-layer stiffness is assumed to be K=10 $\int \frac{E}{2\,L^2(1-\nu)}\,dz$. Fig. 10 depicts the first dimensionless frequency of the system under different boundary conditions. For the system with C-C/C-C boundary conditions, the highest frequency values are associated with the X pattern, while the lower values correspond to the O pattern, across all porosity distributions. On the other hand, when the boundary conditions are changed to S-S/S-S, the higher frequency values correspond to the X and V patterns, whereas the lowest value is linked to the Λ pattern.

To gain insight into how temperature affects the thermal vibration of a system, Table 8 is introduced. The system consists of two porous beams with a porosity of 0.5, reinforced with a medium volume of carbon nanotubes (0.17). The beam geometry is the same as in the previous section, and the stiffness of the beams is 10. Thermal distribution occurs in three different patterns: uniform, linear, and nonlinear. According to the table, there are no differences in the vibration behavior of the system when the temperature of the center or surfaces of the system is increased. However, as the temperature in the environment increases, the frequencies of the system slightly decrease. Moreover, the table shows that there is no significant difference in the vibration behavior of the system between the linear and nonlinear thermal distribution patterns. This indicates that the thermal distribution pattern does not have a significant effect on the thermal vibration behavior of the system. Interestingly, the table also reveals that the frequencies of the system are higher when the temperature increases linearly or nonlinearly compared to a uniform temperature increase. This suggests that when the temperature distribution is not uniform, the thermal vibrations of the system are affected differently than in a uniform temperature distribution.

6. Conclusions

The objective of this study was to examine the dynamic response of a nanocomposite under thermal loading and free vibration. The system consisted of two curved beams with porosity, connected by an elastic mid-layer. Transitional elastic springs were used in the numerical simulations to replace the elastic mid-layer. The homogenous porous beam was composed of steel foam, while the composite section consisted of PMMA as the matrix and SWCNT as the nanofiller. The RoM was employed to determine the equivalent mechanical properties of the nanocomposite. The porosity and CNTs were distributed differently along the beams' height. The GDQ technique was used to discretize the governing differential equations, which were derived based on the FOSDT, to obtain the system's natural frequencies. The results confirmed the correctness and accuracy of the proposed procedure. Additionally, various parameters that influence the vibrational behavior of the system were numerically studied, leading to the following findings:

1- In a single porous curved beam, increasing the R/h ratio and porosity coefficient decreases the system's frequencies. Asymmetric patterns result in higher frequency values than uniform patterns.

2- The frequencies of a single porous curved beam reinforced with CNTs increase with an increase in the volume of SWCNTs.

3- Similar to a single beam, the frequencies of a coupled porous curved beam decrease with an increase in the R/h ratio.

4- The mid-layer stiffness, defined as the ratio of material properties, has no effect on the frequencies of the first mode. However, the frequencies of other modes increase within a specific range of spring stiffness values.

5- The effect of CNT patterns on the frequencies of a coupled porous curved beam was studied, and the results showed that the frequencies were dependent on the boundary conditions and the pattern used.

6- Thermal loading was implemented in governing equations, and three types of patterns were employed for temperature distribution. An increase in temperature caused a decrease in the system's frequencies, and there were no differences between linear and nonlinear distributions.

Acknowledgments

The research of the corresponding author is supported by a grant from Ferdowsi University of Mashhad (N2. 59254)

References

Abediokhchi, J., Kouchakzadeh, M.A. and Shakouri, M. (2013), "Buckling analysis of cross-ply laminated conical panels using GDQ method", *Compos. Part B Eng.*, **55**, 440-446. https://doi.org/10.1016/j.compositesb.2013.07.003.

Akbas, S.D. (2018), "Forced vibration analysis of cracked functionally graded microbeams", *Adv. Nano Res.*, **6**, 39-55. https://doi.org/10.12989/anr.2018.6.1.039

Al-shujairi, M. and Mollamahmutoğlu, Ç. (2018), "Buckling and free vibration analysis of functionally graded sandwich micro-beams resting on elastic foundation by using nonlocal strain gradient theory in conjunction with higher order shear theories under thermal effect", *Compos. Part B Eng.*, **154**, 292-312. https://doi.org/10.1016/j.compositesb.2018.08.103.

Babaei, H. (2022), "Free vibration and snap-through instability of FG-CNTRC shallow arches supported on nonlinear elastic foundation", *Appl. Math. Comput.*, **413**. https://doi.org/10.1016/j.amc.2021.126606.

Babaei, H., Kiani, Y. and Eslami, M.R. (2019), "Large amplitude free vibration analysis of shear deformable FGM shallow arches on nonlinear elastic foundation", *Thin. Wall. Struct.*, **144**, 106237. https://doi.org/10.1016/j.tws.2019.106237.

Batihan, A.Ç. and Kadioğlu, F.S. (2016), "Vibration analysis of a cracked beam on an elastic foundation", *Int. J. Struct. Stabil. Dyn.*, **16**. https://doi.org/10.1142/S0219455415500066.

Berghouti, H., Bedia, E.A.A., Benkhedda, A. and Tounsi, A. (2019), "Vibration analysis of nonlocal porous nanobeams made of functionally graded material", *Adv. Nano Res.*, **7**(5), 351. https://doi.org/10.12989/anr.2019.7.5.351.

Chaabane, L.A., Bourada, F., Sekkal, M., Zerouati, S., Zaoui, F.Z., Tounsi, A., Derras, A., Bousahla, A.A. and Tounsi, A. (2019), "Analytical study of bending and free vibration responses of functionally graded beams resting on elastic foundation", *Struct. Eng. Mech.*, **71**. https://doi.org/10.12989/sem.2019.71.2.185

Chen, D., Yang, J. and Kitipornchai, S. (2016), "Free and forced vibrations of shear deformable functionally graded porous beams", *Int. J. Mech. Sci.*, **108-109**, 14-22. https://doi.org/10.1016/j.ijmecsci.2016.01.025.

Chen, Y., Jin, G., Zhang, C., Ye, T. and Xue, Y. (2018), "Thermal vibration of FGM beams with general boundary conditions using a higher-order shear deformation theory", *Compos. Part B Eng.*, **153**, 376-386. https://doi.org/10.1016/j.compositesb.2018.08.111.

Deng, H., Chen, k., Cheng, W. and Zhao, S. (2017), "Vibration and buckling analysis of double-functionally graded Timoshenko beam system on Winkler-Pasternak elastic foundation", *Compos. Struct.*, **160**, 152-168. https://doi.org/10.1016/j.compstruct.2016.10.027.

Ebrahimi, F. and Farazmandnia, N. (2018), "Vibration analysis of functionally graded carbon nanotube reinforced composite sandwich beams in thermal environmen", *Adv. Aircr. Spacecr. Sci.*, **5**. https://doi.org/10.12989/aas.2018.5.1.107

Ebrahimi, F., Jafari, A. and Selvamani, R. (2020), "Thermal buckling analysis of magneto-electro-elastic porous FG beam in thermal environment", *Adv. Nano Res.*, **8**(1), 83. https://doi.org/10.12989/anr.2020.8.1.083.

Ehyaei, J., Akbarshahi, A. and Shafiei, N. (2017), "Influence of porosity and axial preload on vibration behavior of rotating FG nanobeam", *Adv. Nano Res.*, **5**, 141-169. https://doi.org/10.12989/anr.2017.5.2.141

Eiadtrong, S., Wattanasakulpong, N. and Vo, T.P. (2023), "Thermal vibration of functionally graded porous beams with classical and non-classical boundary conditions using a modified Fourier method", *Acta Mech.*, **234**, 729-750. https://doi.org/10.1007/s00707-022-03401-5.

Elimat, Z.M., Zihlif, A.M. and Avella, M. (2008), "Thermal and optical properties of poly(methyl methacrylate)/calcium carbonate nanocomposite", *J. Experim. Nanosci.*, **3**(4), 259-269. https://doi.org/10.1080/17458080802603715.

Fariborz, J. and Batra, R.C. (2019), "Free vibration of bi-directional functionally graded material circular beams using shear deformation theory employing logarithmic function of radius", *Compos. Struct.*, **210**, 217-230. https://doi.org/10.1016/j.compstruct.2018.11.036.

Fenjan, R.M., Hamad, L.B. and Faleh, N.M. (2020), "Mechanical-hygro-thermal vibrations of functionally graded porous plates with nonlocal and strain gradient effec", *Adv. Aircr. Spacecr. Sci.*, **7**. https://doi.org/10.12989/aas.2020.7.2.169.

Ghandehari, M.A., Masoodi, A.R. and Panda, S.K. (2023), "Thermal frequency analysis of double CNT-reinforced polymeric straight beam", *J. Vib. Eng. Technol.*, 1-17. https://doi.org/10.1007/s42417-023-00865-0.

Ghasemi, A.R. and Mohande, M. (2016), "The effect of finite strain on the nonlinear free vibration of a unidirectional composite Timoshenko beam using GDQ", *Adv. Aircr. Spacecr. Sci.*, **3**(4), 379. https://doi.org/10.12989/aas.2016.3.4.379.

Gholami, R. and Ansari, R. (2018), "Nonlinear harmonically excited vibration of third-order shear deformable functionally graded graphene platelet-reinforced composite rectangular plates", *Eng. Struct.*, **156**, 197-209. https://doi.org/10.1016/j.engstruct.2017.11.019.

Hadji, L. and Avcar, M. (2021), "Nonlocal free vibration analysis of porous FG nanobeams using hyperbolic shear deformation beam theo", *Adv. Nano Res.*, **10**(3), 281. https://doi.org/10.12989/anr.2021.10.3.281

Hamada, T.R., Nakayama, H. and Hayashi, K. (1983), "Free and forced vibrations of elastically connected double-beam systems", *Bull. JSME*, **26**(221), 1936-1942. https://doi.org/10.1299/jsme1958.26.1936.

Han, Z. and Fina, A. (2011), "Thermal conductivity of carbon nanotubes and their polymer nanocomposites: A review", *Prog. Polym. Sci.*, **36**(7), 914-944. https://doi.org/10.1016/j.progpolymsci.2010.11.004.

Hosseini, S.A.H., Rahmani, O., Refaeinejad, V., Golmohammadi, H. and Montazeripour, M. (2023), "Free vibration of deep and

shallow curved FG nanobeam based on nonlocal elasticity", *Adv. Aircr. Spacecr. Sci.*, **10**. https://doi.org/10.12989/aas.2023.10.1.051

Javani, M., Kiani, Y. and Eslami, M.R. (2021), "Application of generalized differential quadrature element method to free vibration of FG-GPLRC T-shaped plates", *Eng. Struct.*, **242**, 112510. https://doi.org/10.1016/j.engstruct.2021.112510.

Jena, S.K., Chakraverty, S. and Malikan, M. (2020), "Vibration and buckling characteristics of nonlocal beam placed in a magnetic field embedded in Winkler–Pasternak elastic foundation using a new refined beam theory: An analytical approach", *Eur. Phys. J. Plus*, **135**(2), 164. https://doi.org/10.1140/epjp/s13360-020-00176-3.

Jouneghani, F.Z., Dimitri, R. and Tornabene, F. (2018), "Structural response of porous FG nanobeams under hygro-thermo-mechanical loadings", *Compos. Part B Eng.*, **152**, 71-78. https://doi.org/10.1016/j.compositesb.2018.06.023.

Kitipornchai, S., Chen, D. and Yang, J. (2017), "Free vibration and elastic buckling of functionally graded porous beams reinforced by graphene platelets", *Mater. Des.*, **116**, 656-665. https://doi.org/10.1016/j.matdes.2016.12.061.

Li, X., Li, L., Hu, Y., Ding, Z. and Deng, W. (2017), "Bending, buckling and vibration of axially functionally graded beams based on nonlocal strain gradient theory", *Compos. Struct.*, **165**, 250-265. https://doi.org/10.1016/j.compstruct.2017.01.032.

Li, Z., Xu, Y. and Huang, D. (2021), "Analytical solution for vibration of functionally graded beams with variable cross-sections resting on Pasternak elastic foundations", *Int. J. Mech. Sci.*, **191**, 106084. https://doi.org/10.1016/j.ijmecsci.2020.106084.

MaraŞ, S. and ŞEnsoy, A.T. (2023), "Estimating the effect of certain manufacturing parameters for fiber laminated composites: A validated DQM model integrated with RSM", *Eng. Anal. Bound. Elem.*, **155**, 169-181. https://doi.org/10.1016/j.enganabound.2023.06.007.

Maraş, S. and Yaman, M. (2022), "Free vibration analysis of fiber-metal laminated composite plates using differential, generalized and harmonic quadrature methods: experimental and numerical studies", *Eng. Comput.*, **39**(6), 2326-2349. https://doi.org/10.1108/EC-08-2021-0490.

Maraş, S. and Yaman, M. (2023), "Investigation of dynamic properties of GLARE and CARALL hybrid composites: Numerical and experimental results", *Eng. Anal. Bound. Elem.*, **155**, 484-499. https://doi.org/10.1016/j.enganabound.2023.06.026.

Maraş, S., Yaman, M., Şansveren, M.F. and Reyhan, S.K. (2018), "Free vibration analysis of fiber metal laminated straight beam", *Open Chem.*, **16**(1), 944-948. https://doi.org/10.1515/chem-2018-0101.

Oniszczuk, Z. (2000), "Free transverse vibration of elastically connected simply supported double-beam complex system", *J. Sound Vib.*, **232**(2), 387-403. https://doi.org/10.1006/jsvi.1999.2744.

Ramteke, P.M. and Panda, S.K. (2023), "Computational modelling and experimental challenges of linear and nonlinear analysis of porous graded structure: A comprehensive review", *Arch. Comput. Methods Eng.*, **30**(5), 3437-3452. https://doi.org/10.1007/s11831-023-09908-x.

Rao, S.S. (1974), "Natural vibrations of systems of elastically connected Timoshenko beams", *J. Acoust. Soc. Am.*, **55**(6). https://doi.org/10.1121/1.1914690.

Rezaiee-Pajand, M. and Rajabzadeh-Safaei, N. (2016), "Static and dynamic analysis of circular beams using explicit stiffness matrix", *Struct. Eng. Mech.*, **60**. https://doi.org/10.12989/sem.2016.60.1.111.

Rezaiee-Pajand, M. and Masoodi, A.R. (2019), " Analyzing FG shells with large deformations and finite rotations", *World J. Eng.*, **16**(5) 636-647. https://doi.org/10.1108/WJE-10-2018-0357.

Roberts, A.P. and Garboczi, E.J. (2002), "Computation of the linear elastic properties of random porous materials with a wide variety of microstructure", *Proceedings of the Royal Society A*, **458**. https://doi.org/10.1098/rspa.2001.0900.

Sahmani, S. and Safaei, B. (2022), "Nonlinear three-dimensional oscillations of probabilistic reinforced nanocomposite shells at microscale via modified strain gradient meshfree formulations", *Proceedings of the Institution of Mechanical Engineers, Part C: J. Mech. Eng. Sci.*, 09544062221142144. https://doi.org/10.1177/09544062221142144.

Salehi Kolahi, M.R., Moeinkhah, H. and Rahmani, H. (2021), "Numerical study of the non-linear vibrations of electrically actuated curved micro-beams considering thermoelastic damping", *Commun. Nonlinear Sci. Numer. Simul.*, **103**, 106009. https://doi.org/10.1016/j.cnsns.2021.106009.

Seelig, J. and Hoppmann, I. (1963), *Impact on an Elastically Connected Double Beam System*, Rensselaer Polytechnic Inst Troy, New York, U.S.A.

Shen, H.S. and Xiang, Y. (2013), "Nonlinear analysis of nanotube-reinforced composite beams resting on elastic foundations in thermal environments", *Eng. Struct.*, **56**. https://doi.org/10.1016/j.engstruct.2013.06.002.

Shu (1991), *Generalized differential-integral quadrature and application to the simulation of incompressible viscous flows including parallel computation*, University of Glasgow

Shu (2000), *Differential Quadrature and Its Application in Engineering*, Springer, Berlin.

Sobhani, E. and Masoodi, A.R. (2021), "Natural frequency responses of hybrid polymer/carbon fiber/FG-GNP nano-composites paraboloidal and hyperboloidal shells based on multiscale approaches", *Aerosp. Sci. Technol.*, **119**, 107111. https://doi.org/10.1016/j.ast.2021.107111.

Sobhani, E. and Masoodi, A.R. (2023), "Differential quadrature technique for frequencies of the coupled circular arch–arch beam bridge system", *Mech. Adv. Mater. Struct.*, **30**(4), 770-781. https://doi.org/10.1080/15376494.2021.2023920.

Song, Z.G., Zhang, L.W. and Liew, K.M. (2016), "Vibration analysis of CNT-reinforced functionally graded composite cylindrical shells in thermal environments", *Int. J. Mech. Sci.*, **115-116**, 339-347. https://doi.org/10.1016/j.ijmecsci.2016.06.020.

Tang, H., Li, L. and Hu, Y. (2018), "Buckling analysis of two-directionally porous beam", *Aerosp. Sci. Technol.*, **78**, 471-479. https://doi.org/10.1016/j.ast.2018.04.045.

Tang, Y. and Ding, Q. (2019), "Nonlinear vibration analysis of a bi-directional functionally graded beam under hygro-thermal loads", *Compos. Struct.*, **225**, 111076. https://doi.org/10.1016/j.compstruct.2019.111076.

Tlidji, Y., Benferhat, R., Trinh, L.C., Tahar, H.D. and Abdelouahed, T. (2021), "New state-space approach to dynamic analysis of porous FG beam under different boundary conditio", *Adv. Nano Res.*, **11**(4), 347. https://doi.org/10.12989/anr.2021.11.4.347.

Tornabene, F. and Dimitri, R. (2018), "A numerical study of the seismic response of arched and vaulted structures made of isotropic or composite materials", *Eng. Struct.*, **159**, 332-366. https://doi.org/10.1016/j.engstruct.2017.12.042.

Vu, H.V., Ordóñez, A.M. and Karnopp, B.H. (2000), "Vibration of a double-beam system", *J. Sound Vib.*, **229**(4), 807-822. https://doi.org/10.1006/jsvi.1999.2528.

Xiaobin, L.I., Shuangxi, X.U., Weiguo, W.U. and Jun, L.I. (2014), "An exact dynamic stiffness matrix for axially loaded double-beam systems", *Sadhana*, **39**(3), 607-623. https://doi.org/10.1007/s12046-013-0214-5.

Yas, M.H. and Samadi, N. (2012), "Free vibrations and buckling

analysis of carbon nanotube-reinforced composite Timoshenko beams on elastic foundation", *Int. J. Pres. Ves. Pip.*, **98**, 119-128. https://doi.org/10.1016/j.ijpvp.2012.07.012.

Yu, C., Shi, L., Yao, Z., Li, D. and Majumdar, A. (2005), "Thermal conductance and thermopower of an individual single-wall carbon nanotube", *Nano Lett.*, **5**(9), 1842-1846. https://doi.org/10.1021/nl051044e.

Zhang, P., Schiavone, P. and Qing, H. (2022), "Stress-driven local/nonlocal mixture model for buckling and free vibration of FG sandwich Timoshenko beams resting on a nonlocal elastic foundation", *Compos. Struct.*, **289**, 115473. https://doi.org/10.1016/j.compstruct.2022.115473.

Zhao, X., Chen, B., Li, Y.H., Zhu, W.D., Nkiegaing, F.J. and Shao, Y.B. (2020), "Forced vibration analysis of Timoshenko double-beam system under compressive axial load by means of Green's functions", *J. Sound Vib.*, **464**, 115001. https://doi.org/10.1016/j.jsv.2019.115001.

CC